The 2018 Structures Congress (Structures18)
Songdo Convensia, Incheon, Korea, August 27 - 31, 2018

Research on Seismic Performance of a Separated Structure System

Hongbo Liu[1a], Yan Zhao [*2,3], Siyuan Chen [3], Yongjiang Zhao[1] , Dongdong Tao[1] and Yansong Wang[3]

[1]School of Civil Engineering and Architecture, Heilongjiang University, Harbin 150080, China;
[2]Key Laboratory of Earthquake Engineering and Engineering Vibration, Institute of Engineering Mechanics, China Earthquake Administration, Harbin 150080, China;
[3]School of Civil Engineering and Architecture, Jiamusi University, Jiamusi 154007, China

(Received , Revised , Accepted)

Abstract. In order to compare the seismic performance of a separated structure (SS) system with a rigid steel-frame structure (RS), the dynamic responses of both them were calculated using the dynamic elastoplastic analysis method and the static elastoplastic analysis method (Pushover). Through the investigation of the displacement, acceleration response and capacity curve, the dynamic response laws were obtained. Studies show that the natural vibration frequency of the SS is larger than that of the RS, which indicates that the former has a higher lateral stiffness than the latter. Under the same ground motion, the maximum displacement in the SS is smaller than the RS , indicating that the braces in SS control effectively the lateral deformation of the structure; the braces make the deformation of the structure more uniform; the plastic hinges of the SS are mostly concentrated in the bottom two floors, and even with the full section yielding of beams and braces, it can still resist a certain level of horizontal load, indicating that this SS system has a strong safety reserve.

Keywords: separated structure; rigid steel-frame structure; seismic response; seismic performance; time-history analysis; Pushover analysis

1. Introduction

Multi-story or high-rise steel-structure buildings often use the framework structure system, mainly resisting vertical and horizontal loads through the flexural capacity of beams and columns. The lateral stiffness resistance of the frame structure is relatively small, when the lateral load is large, the section size of the beam or column is often used to increase the lateral stiffness resistance and bearing capacity of the overall structure, though it brings larger economic losses (Foulad 2015). In order to solve this problem, after an in-depth analysis of the mechanical characteristics of multi-high-rise steel-structure buildings, we proposed a new type of structural system called a separated structural system, in which horizontal loads are braced by structural braces. The braces are arranged in different positions of the structure, and they do not reach the yield at the same time, so that the structure has a high redundancy. The vertical loads are borne by the bent structure, and the beams, the columns, and the braces are connected to each other through hinge points, which can effectively avoid the occurrence of brittle failure of the nodes (Liuand Lan 2016). The concrete floor and the steel girder are combined to give full play to the material properties of each member. The lateral load is braced by using axially loaded members instead of bending members, which can greatly reduce the bending moment experienced by the columns. The beams are simply braced on the columns at both ends. Therefore, variable cross-section composite

∗Corresponding author, Associate Professor, E-mail: zhaoyan_hit@163.com
[a] Full Professor, E-mail: HLiu@hlju.edu.cn

beams can be used(Kim and Seo 2004, Liu *et al*.2015, Vasdravellis *et al*.2015). The separated structural systems emphasize on the separation of bearing functions rather than the separation of geometrical positions. It has the advantages of clear load transfer path, good economics, and avoiding brittle failure at both ends of the column (Binnur and Secil 2005, Piotr *et al*. 2001, Gross 1998).

The dynamic elastoplastic time history analysis method consists in building a dynamic equation based on the structural nonlinear restoring force model. Then, the acceleration time-history of the seismic record was entered into the structure. The step-by-step integral method was used to solve the dynamic equation for obtaining the structure displacement, velocity, and acceleration time-history response. With this method, the influence of time can be considered, and the seismic response and internal force changes of the structure in the elastic and non-elastic phases under the action of ground motion is described, and the whole process of cracking, yielding, damaging, and collapsing of structural members is reflected (Torii and Machado 2012). The Pushover is a method that uses the non-linear characteristics of the structural material to evaluate the mechanical property of the structure from the elastic state and the elastoplastic state to the ultimate state (Reza and Mohsenali 2018, Fayaz and Mirjalili 2018, Li *et al*.2017). The Pushover is simpler than the dynamic elastoplastic time-history analysis method. It does not require the use of the restoring force model and input of ground motion records and not only reflects the overall deformation of the structure mainly reacted to the first vibration mode and the local plastic deformation mechanism (Liu *et al*.2018, Yin *et al*.2018, Gupta and Kunnath 2000), but more importantly, the Pushover can also predict and analyze the destroy forms of the structure upon rare earthquakes with a good grade of accuracy (Yang *et al*.2017, Phaiboon 2014). In this paper, the dynamic elastoplastic time-history analysis method and the Pushover are used to analyze the SS system, so as to evaluate the seismic performance of this kind of structural system and provide a theoretical basis for the structural anti-seismic design and engineering application.

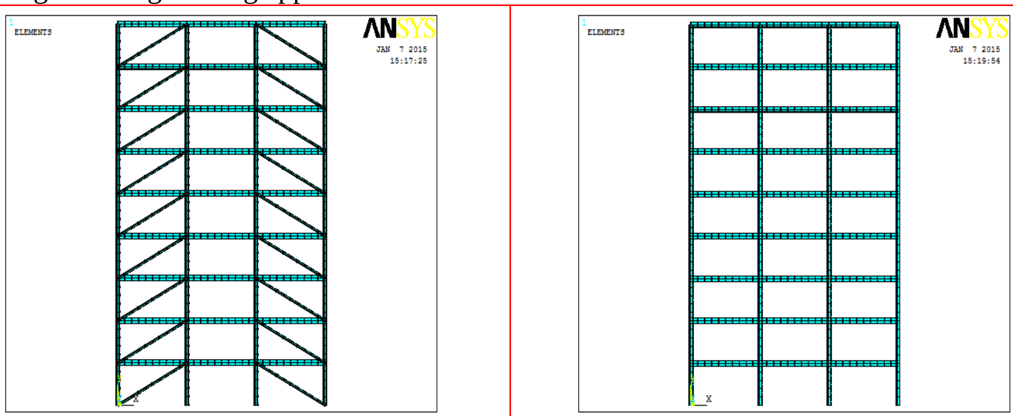

(a) the separated steel-structure (b) the rigid steel-frame structure

Fig. 1 Full-scale finite element model

2. Structural Model

In order to evaluate the seismic performance of the SS, according to the principle of the structure form corresponding to the steel consumption, the single-frame full-scale finite element model was established using a SS and a RS, shown in Fig. 1. The model structure has a total of 9 floors and 3 spans, with a floor height of 3 meters and a span of 6 meters. The SS uses the columns with dimensions of H300 mm × 300mm × 10 mm × 15mm; beams with the dimensions of H400 mm × 200 mm × 8 mm × 13 mm; braces use variable cross-section box type of sections, with middle section size of 300 mm × 300 mm × 8 mm, and end section size of 150 mm × 150 mm × 8 mm. The RS uses the columns of H350 mm × 350 mm × 12 mm × 19 mm, and beams of H400 mm × 200 mm × 8 mm × 13 mm.

3. Modal Analysis

By using the ANSYS finite element analysis software, a modal analysis was conducted on the structure to obtain the structure's natural vibration frequency and vibration mode, as shown in Fig. 2. The first natural vibration frequency of the SS f_1 = 0.81Hz and the first natural vibration frequency of the RS f_1 = 0.44Hz. The former's natural vibration frequency is higher than the latter's, indicating that the former has a lateral stiffness resistance larger than that of the latter.

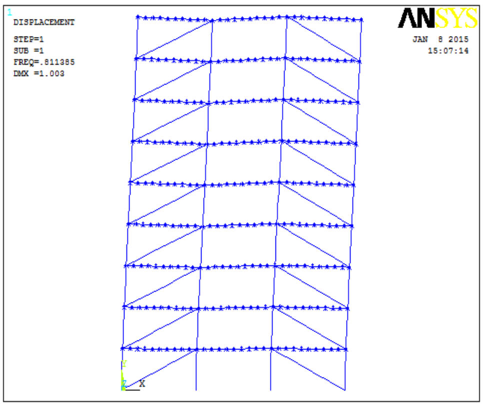

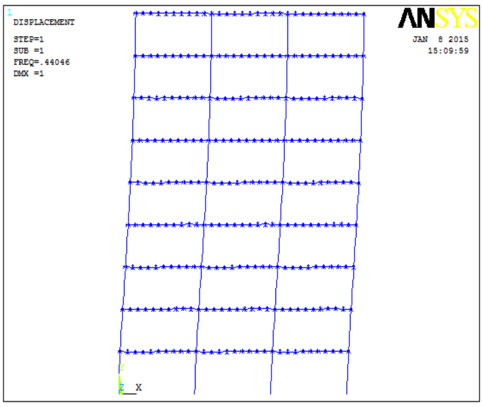

(a) the first mode of the SS (f_1=0.81Hz)

(b) the first mode of the RS (f_1=0.44Hz)

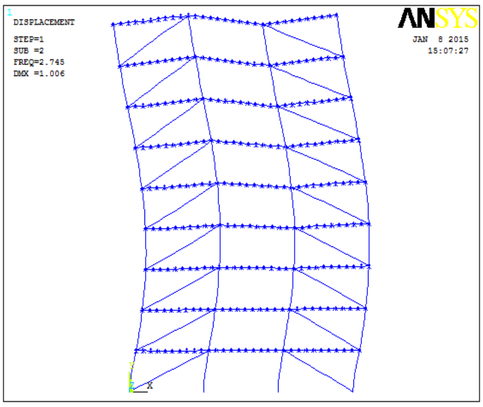

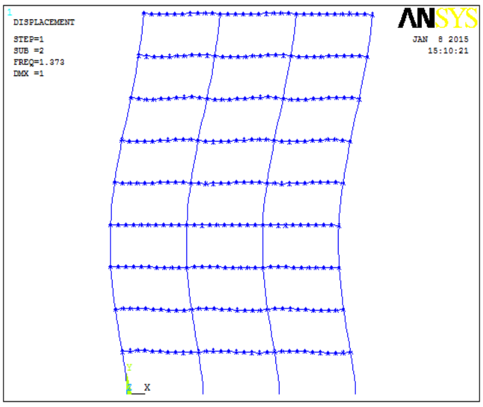

(c) the second mode of SS (f_2=2.74Hz)

(d) the second mode of the RS (f_2=1.37Hz)

Fig. 2 the mode of the structure

4. Dynamic Elastoplastic Time-History Analysis

The dynamic elastoplastic time-history analysis on the structure was performed using the ANSYS finite element software. BEAM188 elements were used for the beams, the columns, and the braces in the structure. The dead load and the variable load were converted into masses and applied to the nodes. The MASS21 element was used for simulation. With the gravity load taken into account, the structural floor dead load is 3.5kN/m^2, the live load is 2.0kN/m^2, and the load between the beams is 18.0kN/m. The materials of the member were simulated with the bilinear follow-up hardening model and the Von Mises yield criterion. When the material enters the reinforcement phase, the nonlinearity and the geometric nonlinearity were considered, so the initial bending of 1/1000 of the rod was applied to the brace. Rayleigh damping was selected, and the supposed damping ratio was ξ = 0.02. The steel used for each member was Q235 steel. The steel has an elastic modulus of E = 2.06×10^{5}MPa, a tangent modulus G = 0.02E, a Poisson's ratio v = 0.3, and a density of 7850 kg/m^3. The column base of the structure has a rigid connection with the ground. First, the model structure was calculated and compared to the experimental results to verify the correctness of the modeling method, selected parameters, material constitution, boundary conditions, etc. Then the seismic response analysis of the SS was conducted to examine the aseismic capacity of this structural system.

4.1 Analysis on the Displacement Response of the Structure

The four ground motion records of LOMA-207, EL Centro-180, TAFT, and LAMAP-A0100 were input into the established model structure. The calculation results of the site geological data of the stations corresponded to the site conditions of Class I, II, III, and IV in China. The input ground-motion intensities were PGA=220 gal and PGA=400 gal, respectively, being used to simulate the rare earthquake with intensity Ⅶ and Ⅷ. The maximum value of the absolute value was extracted from the displacement time-history curves of each floor and the displacement envelope diagram and the inter-story drift of each floor are shown in Fig. 3. From Fig. 3(a), it can be seen that the horizontal displacement of the structure gradually increased with the increase of the floor height, and the SS increased almost linearly. The RS increased non-linearly under the LOMA and EL-Centro ground motion, indicating the displacement response of the upper structure was larger, being the stiffness of the SS was larger as well. However, the maximum displacement of each floor of the SS under the four types of ground motion was smaller than that of the RS, indicating the former's lateral stiffness resistance was larger, and the brace in the structure effectively controlled the lateral deformation of the structure. From Fig. 3(b), it can be seen that in the RS, as the floor height increased, the inter-story drift of the structure first increased and then decreased, showing obvious points of inflection, especially under the LOMA ground motion, the inter-story drift from the 2nd floor to the 4th floor was very large, indicating that the high-order mode has a larger effect on the structure; in the SS, with the increase of the floor height, the inter-story drift almost increased linearly without showing the phenomenon of the RS, indicating that the brace increased the stiffness of the structure and made the deformation of the structure more uniform. Under the four types of ground motions, the inter-story drifts of the SS from the 5th floor to the 8th floor were all smaller than those of the RS, while the part from the 6th floor to the 9th floor had the opposite condition, proving that the brace had a larger effect on the lower part of the structure and could control the lateral movement of the lower structure more effectively. From Fig. 3 (a) and Fig. 3 (b), it can be seen that whether PGA=220 gal or PGA=400 gal, the displacement response and the inter-story drift caused by the LOMA ground motion on the condition of Class I site were significantly greater than those of those caused by the LAMAP ground motion on Class IV. That was more evident in the RS, indicating that the natural vibration period of the structure was closer to the predominant period of Class I site.

4.2 Analysis on the Acceleration Response of the Structure

The maximum value of the absolute value was extracted from the acceleration time-history curve of each floor, to obtain the corresponding acceleration envelope diagram of each floor, seen in Fig. 4. It can be seen that with the increase of the floor height, the acceleration response of the structure gradually increased, and the acceleration responses of the structure above the 5th floor were larger than the input earthquake intensity. When PGA=220 gal, the acceleration response of the SS almost linearly increased, and there was a small number of points of inflection in the RS. The acceleration response of the SS of most floors was lower than that of the RS. When PGA = 400 gal, in the lower floors of the structure, the acceleration response of the SS was lower than that of the RS, and the former in the upper part of the structure was larger than the latter, and the intersection of the two is basically in the 5-7 floors, indicating the brace controlled effectively the dynamic response of the lower part of the structure; the acceleration response of the SS presented a small number of points of inflection, while the acceleration response of the RS showed an obvious S-shape.

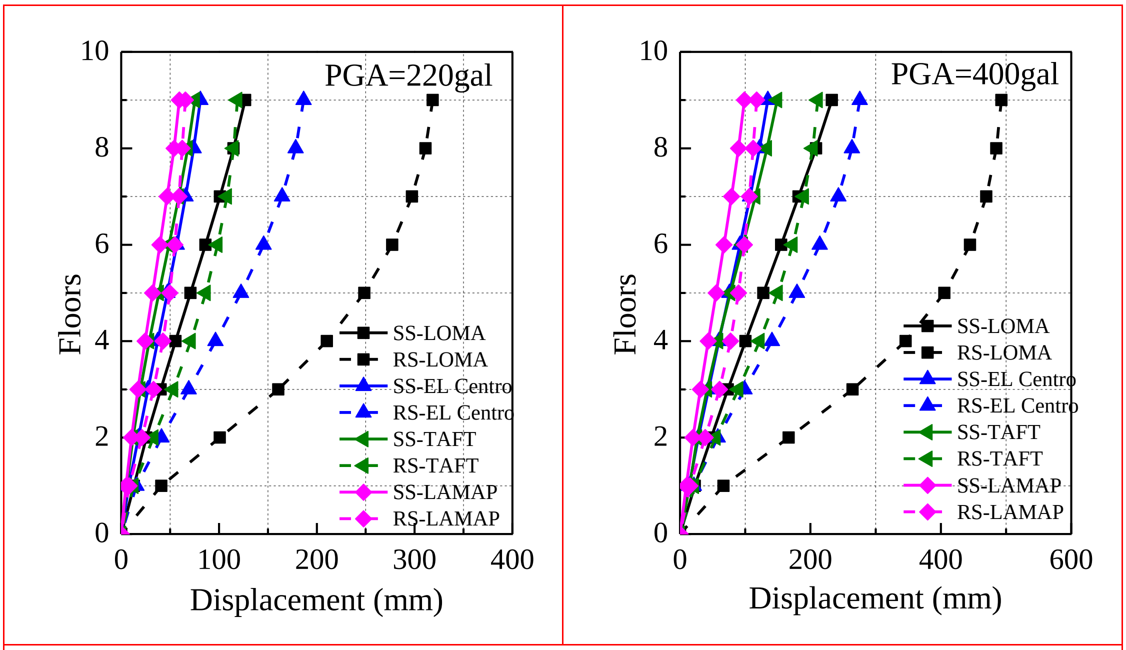

(a) Maximum displacement of each floor of the structure

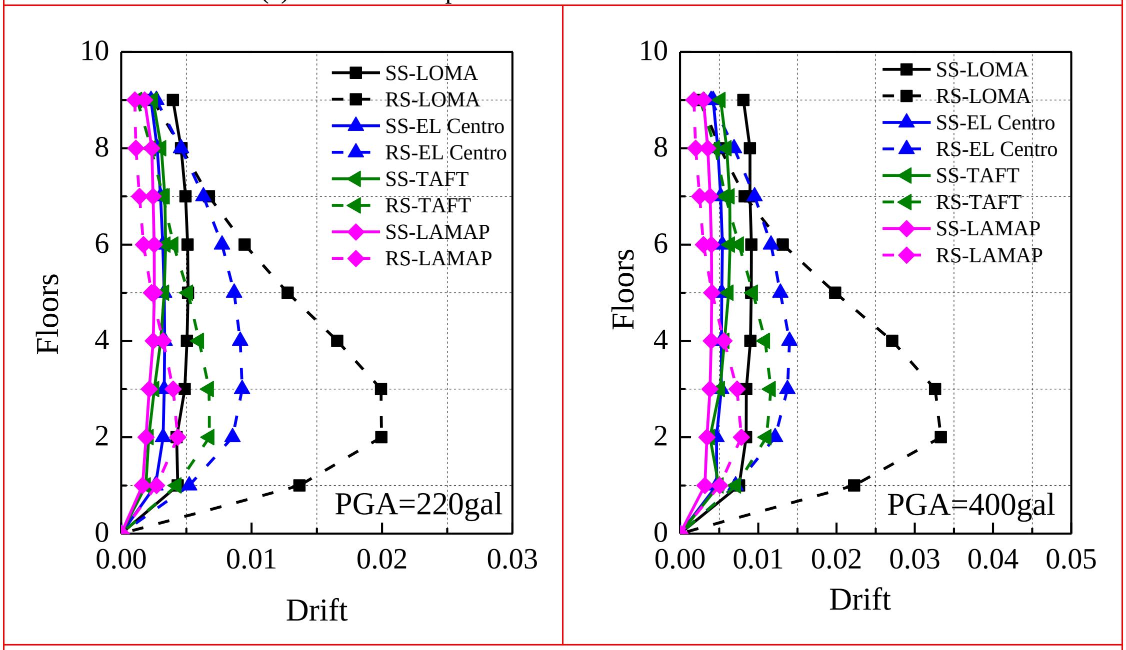

(b) the inter-story drift of the structure

Fig. 3 the maximum displacement and the inter-story drifts of each floor in the structure

5. Static Elastoplastic Analysis (Pushover)

5.1 Capacity Curve

The capacity spectrum curve is the acceleration-displacement response spectrum curve. By applying lateral loads to the model structure until the structure was destroyed, the Pushover curve was drawn with the vertex displacement as the horizontal axis and the base shear force as the vertical axis. The multi-degree-of-freedom system was changed to equivalent single degree-of-freedom system according to a certain deformation mode (usually the basic mode). The base shear V_b was converted to the spectral acceleration S_a, the vertex displacement U_n into the spectral displacement S_d, forming the capacity spectrum curve of the structure (Yin 2018). See Eq. (1) for the transition process.

$$S_a = \frac{V_b}{M_1^*} \qquad S_d = \frac{U_n}{\gamma \varphi_{n1}^2} \tag{1}$$

$$M_1^* = \frac{(\sum_{i=1}^{n} m_i \varphi_{i1})^2}{\sum_{i=1}^{n} m_i \varphi_{i1}^2} \qquad \gamma = \frac{\sum_{i=1}^{n} m_i \varphi_{i1}}{\sum_{i=1}^{n} m_i \varphi_{i1}^2}$$

Where: V_b-- base shear; U_n--vertex displacement; γ -- the first mode participation coefficient of the structure; M_1*--effective quality; m_i--the quality of the mass point on the i^{th} floor; φ_{i1}--amplitude of the mass point on the i^{th} floor in the first mode.

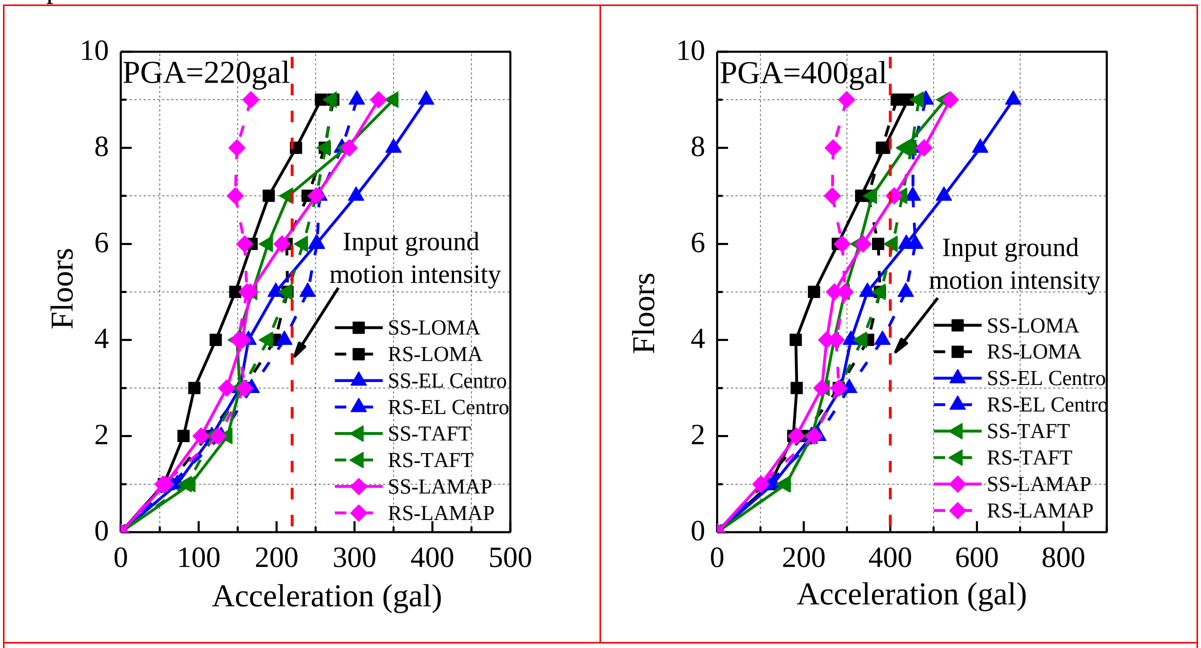

Fig. 4 the maximum acceleration of each floor in the structure

The distribution pattern of lateral loads is one of the key issues for Pushover. Many scholars at home and abroad have done their own research and put forward a variety of lateral load distribution methods, of which the adaptive lateral load and the fixed lateral load have been widely recognized (Gupta and Kunnath 2000,Yang *et al*.2017). Studies have shown that under the ground motion, for the structures that are more affected by the first mode and less affected by other modes, the effects of high-order modes on the structure can be ignored. In this paper, the Pushover curve was obtained by applying the lateral force onto the structure according to the deformation mode of the structural model under the first vibration mode, and the Pushover curve was transformed into the capacity curve. The Pushover curve and the capacity curve of the SS and the RS are shown in Fig. 5. It can be seen that the former had a large lateral stiffness resistance and a strong lateral resistance capacity in the elastic stage, showing a good ductility and a strong deformability in the yielding stage, which is more favorable to the dissipation of energy.

5.2 Demand Curves and Performance Points

According to the capacity curve, the weak story and the possible failure modes of the structure can be roughly judged, but it is required to use the demand curve to solve the structure's target displacement and evaluate the aseismic performance of the structure. The demand curve is the maximum seismic response value of the structure obtained by inputting the given ground motion acceleration time-history into the single-degree-of-freedom system of the natural vibration frequency distributed over a certain range. The displacement-acceleration response curve was plotted with the displacement response of the structure as the horizontal axis, and the acceleration response as the vertical axis (i.e. demand curve) (Phaiboon 2014). There are multiple ways to establish the demand curve. The commonly used method is the equivalent high damping elastic response spectrum proposed in ATC-40 and the improved capacity spectrum method proposed by Chopra. The curves established with improved capacity spectrum method are divided into the constant-ductility strength demand curve and the constant-strength ductility demand curve. Some scholars have found that, between the two methods, the establishment of the ductility demand spectrum is the simpler, and the predicted target displacement is more conservative (Fajfar 1999) with the ductility spectrum. Therefore, the ductility demand spectrum is used to predict the target displacement in this paper.

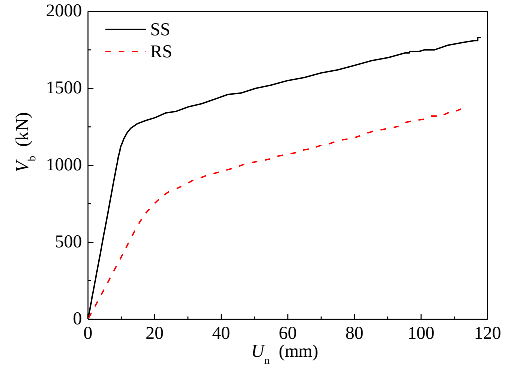

(a) Pushover Curves

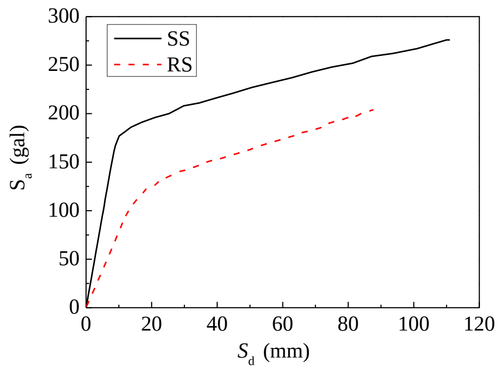

(b) Capacity Curves

Fig. 5 Pushover curves and Capacity curves

Similarly, four ground motion records of LOMA-207, EL Centro-180, TAFT, and LAMAP-A0100 were selected. The input ground-motion intensities were PGA=220 gal and PGA=400 gal, respectively. The Seismo Signal seismic record analysis software was used to obtain the demand curve. And the demand curve was drawn in the same graph with the capacity curve. The intersection of the two curves is the performance point. The coordinate values of the performance points of the SS and the RS under various operating conditions are shown in Table 1. It can be seen from the Table 1 that the spectrum displacement of the SS is lower than that of the RS in the same working conditions. The spectrum acceleration of the former is greater than the latter, and it can be seen that the lateral stiffness resistance of the SS is larger, so the lateral displacement of the structure is effectively controlled, and the structure has a strong lateral resistance capacity.

Table 1 Coordinate values of performance point

Working Conditions	Separated Structure		Rigid Steel-Frame Structure	
	S_d/mm	S_a/gal	S_d/mm	S_a/gal
LOMA-207，PGA=220gal	120	184	290	140
LOMA-207，PGA=400 gal	200	197	450	153
EL Centro-180，PGA=220 gal	80	164	140	103
EL Centro-180，PGA=400 gal	130	186	210	126
TAFT，PGA=220 gal	70	136	110	91
TAFT，PGA=400 gal	130	185	180	120
LAMAP-A0100，PGA=220 gal	60	144	60	53

LAMAP-A0100，PGA=400 gal	140	187	110	92

5.3 Displacement Envelope Diagram

The displacement of the multi-degree-of-freedom structure was inversely calculated according to the performance point, and the displacement of each floor and inter-story drift were obtained. The displacement envelope diagrams obtained by dynamic elastoplastic time-history analysis and Pushover are shown in Fig. 6. It can be seen in Fig. 6 that the displacement envelope diagrams obtained by the dynamic elastoplastic time-history analysis method and the Pushover method were roughly the same in shape and similar in value, no matter whether it was for the SS or the RS, indicating that the Pushover method can accurately calculate the response of this type of structure under an ground motion action. The maximum displacement of each floor calculated by the Pushover method was slightly larger than that obtained by the time-history analysis method. It may be because the influence of the high-order vibration type on the structure was not taken into account in the Pushover analysis method. Compared to the RS, the results between the dynamic elastoplastic time-history analysis and the Pushover analysis of the SS showed a big difference in, indicating that the SS is more affected by the higher-order vibration modes. According to the comparison of the maximum horizontal displacements of each floor in a SS and in a RS, under the effect of LOMA-207 ground motion, the displacement of the former was smaller than that of the latter, and the difference between the two was large. Under the action of LAMAP-A0100 ground motion, the displacement of the former was very similar to that of the latter, and the difference of the two was very small. Under the action of EL Centro-180 and TAFT ground motions, the displacement difference between the two was moderate. The LOMA-207 ground motion station is in Class I site condition, and the LAMAP-A0100 ground motion station is in Class IV site condition, indicating that the brace in the SS improved the overall stiffness of the structure. In the SS, with the increase of the floor height, the maximum displacement of each floor increased almost linearly, while in the RS, it showed a curve increase, indicating that the SS can effectively control the deformation of the weak parts of the intermediate floors, thus matching the conclusion obtained through the dynamic elastoplastic time-history analysis, proving that the results of the dynamic elastoplastic time-history analysis method are consistent with those obtained by the Pushover method.

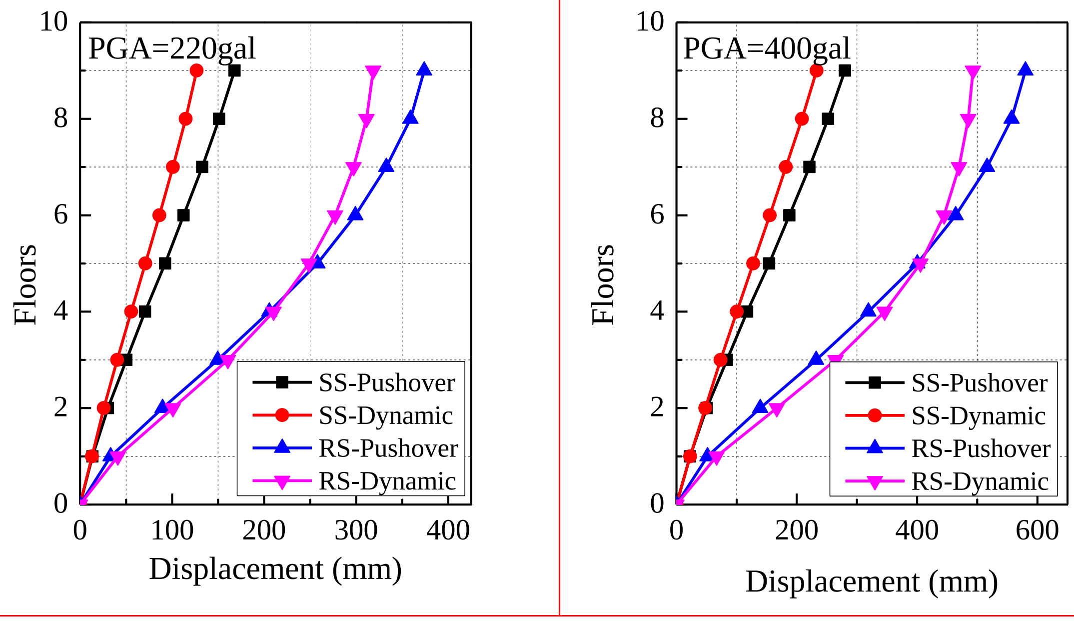

(a) LOMA-207

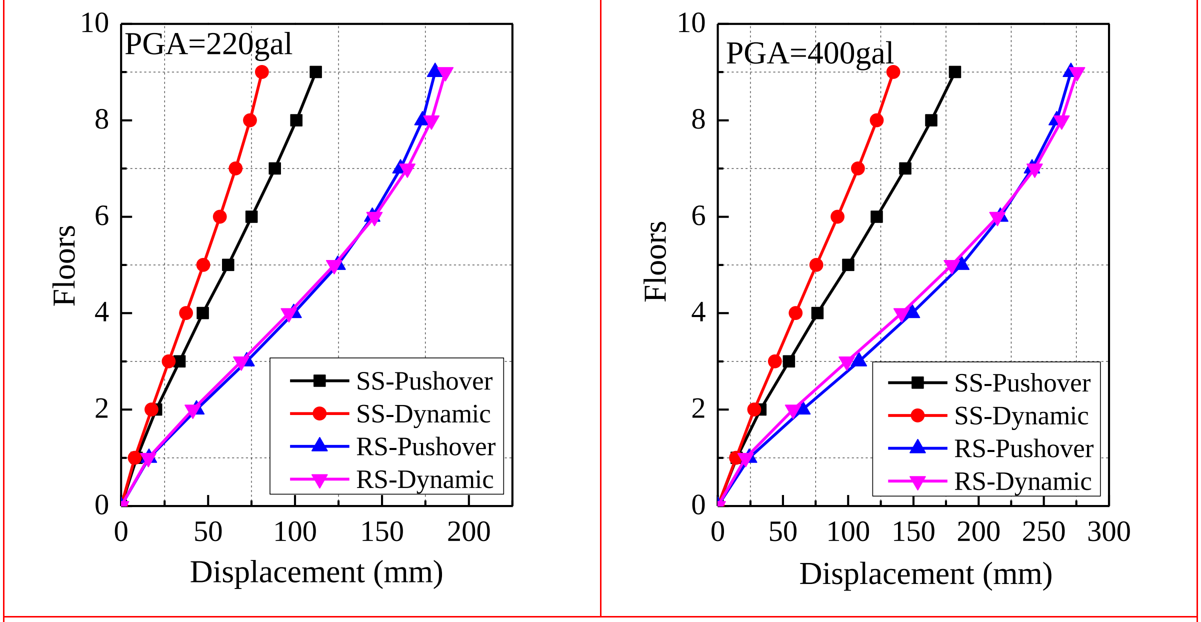

(b) EL Centro-180

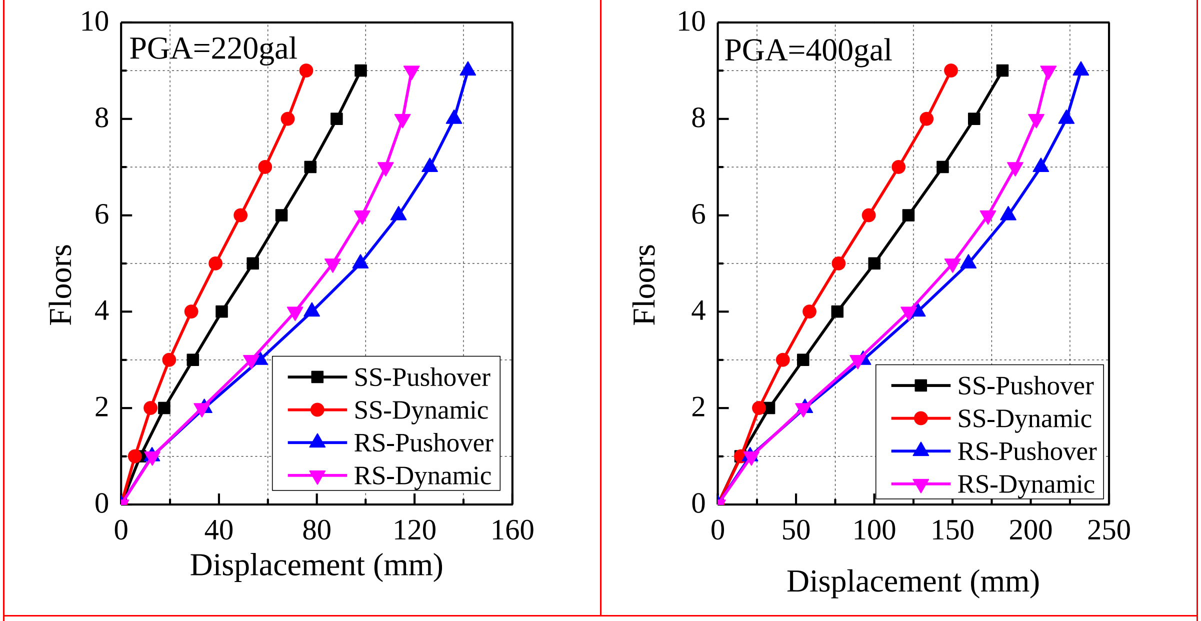

(c) TAFT

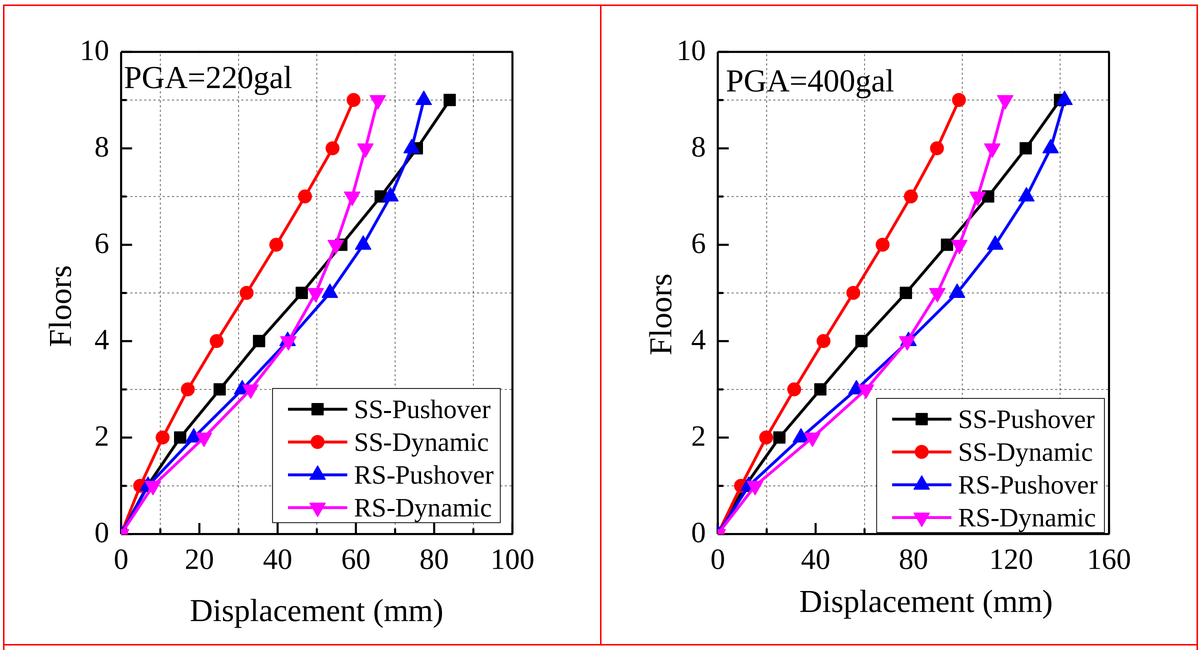

(d) LAMAP-A0100

Fig. 6 Envelope diagram of displacement

5.4 Distribution of Plastic Hinges

The Pushover method can examine the non-linearity of the structure through the plastic hinges. The position and sequence of the plastic hinges reflect the structure's stress state, the member's yield process and the failure mode to some extent. The plastic hinge distribution in the SS and the RS is shown in Fig. 7.

From Fig. 7 (a), it can be seen that when the lateral load V_b=1120 kN, the plastic hinge began to appear at the column base of the SS; as the lateral load increased, the plastic area gradually increased as well. When V_b =1310 kN, the tensile brace of the first floor entered full-section yielding, and the plastic hinges began to form on the columns of the first and second floors. When V_b =1,500 kN, the plastic area on the columns of the first and second floors gradually increased, and the steel beams of the first and second floors also began to enter the plasticity state; when V_b =1700 kN, the tensile brace of the second floor entered full-section yielding, and the column top and column bottom of the third floor formed plastic hinges; finally, the structural calculation was of non-convergent overflow, and no new plastic hinge appeared.

From Fig. 7(b), it can be seen that when the lateral load V_b =642 kN, the plastic hinges began to appear at the column base of the intermediate span of the RS and at the beam end of the intermediate span of the first floor. With the gradual increase of the lateral load, the number of plastic area gradually increased, and the position of the plastic hinges gradually moved up; when V_b =810 kN, plastic hinges appeared at the beam-column joints from the first floor to the fourth floor; when V_b =1010 kN, the plastic hinges appeared at the beam-column joints from the fifth floor to the seventh floor; finally, the structural calculation was of non-convergent overflow, and no new plastic hinge appeared.

Comparing the appearance process and development sequence of the plastic hinges under the lateral load between the SS and the RS, it can be concluded that: (1) In general, the number of plastic hinges in the SS is lower than that of the RS. The plastic hinge is located close to the lower floor of the structure. This is because beams, columns, and braces are hinged to each other in the separate structure, and the beam and brace are both axially loaded members, not generating end bending moments or forming plastic hinges; and (2) When the lateral force reaches a certain level, although the beam and the brace of the SS have full-section yielding, they can still resist the horizontal load, indicating the SS meets the requirements of multi-aseismic resistance aim, avoiding the danger of continuous collapse of the structure due to the buckling of some members; and (3) according to the force-bearing characteristics of the SS, as well as the force characteristics of the two-force rods, i.e. when the rod is applied with pressure, the bending moment at the end of the rod member is small, while the bending moment at the middle is large. The beam and the brace are designed as variable cross-section members with larger midsection size and smaller end size, so as to fully utilize the mechanical properties of the material and save steel; and (4) the plastic hinges of SS are mostly concentrated in the two bottom floors, so the two bottom floors are the weakest part of the structure, and the those should be properly reinforced during design.

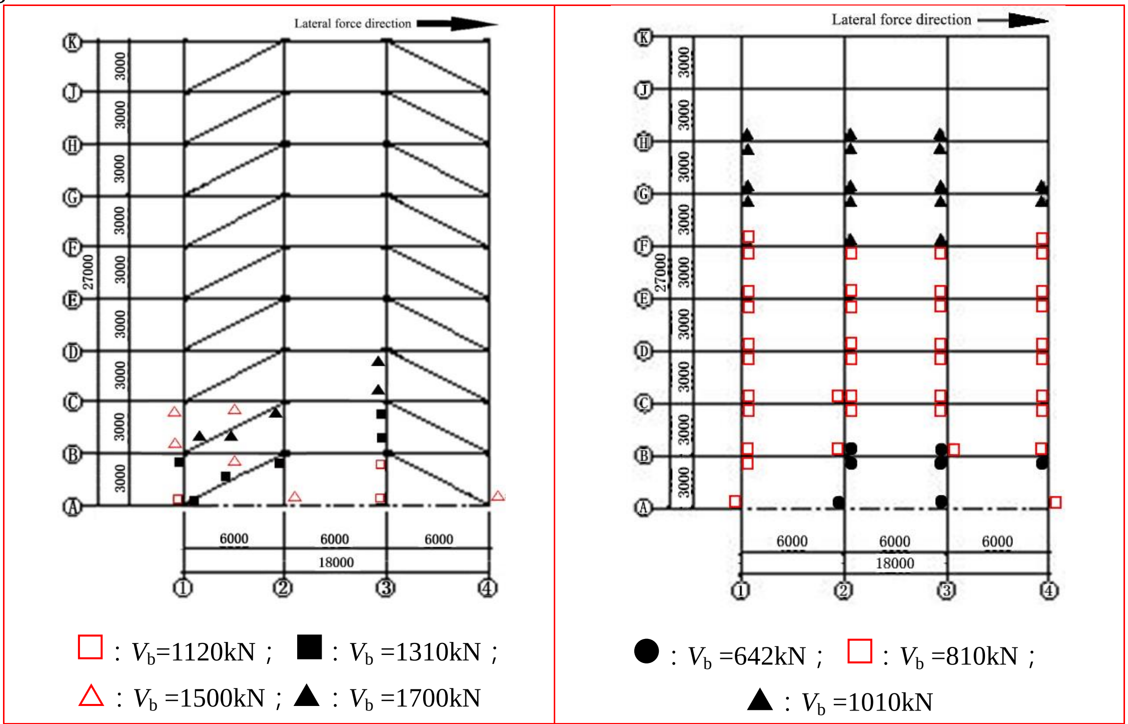

(a) the separated structure | (b) the rigid steel-frame structure

Fig. 7 the distribution of the plastic hinges

6. Conclusion

The seismic performance analysis of the SS and the RS was carried out using the dynamic elastoplastic time history analysis method and the Pushover method respectively. The four typical seismic records of LOMA-207, EL Centro-180, TAFT, and LAMAP-A0100 were selected and the station classes corresponded to the site conditions of Class I, II, III, and IV in China. The ground-motion intensities were PGA=220 gal and PGA=400 gal, respectively, which were used to simulate the rare earthquake with intensity Ⅶ and Ⅷ. The structural modes were analyzed, and the dynamic response laws of the structure were obtained by using the recorded displacement time-history and the acceleration time-history. By observing the distribution and development characteristics of the plastic hinges, the force-bearing performance of the SS and the RS were compared. The following conclusions have been drawn.

- The natural vibration frequency of the SS is greater than that of the RS, indicating that the former has a larger lateral stiffness resistance than the latter.
- Under the same ground motion, the maximum displacement of each floor in the SS is smaller than that of the RS, indicating that the former has a larger lateral stiffness resistance than the latter and the

brace in the structure effectively controls the lateral deformation of the structure. With the increase of the floor height, in the SS, the inter-story drift increases almost linearly, however, in the RS, the inter-story drift first increases and then decreases, showing obvious inflection points. It shows that the brace increases the stiffness of the structure and makes the deformation of the structure more uniform.

- When PGA = 220 gal, the acceleration response of the SS increases almost linearly, and there is a slight point of inflection in the RS; when PGA = 400 gal, the acceleration response of the SS presents a slight point of inflection. However, the acceleration response of the RS is obviously S-shaped, indicating that the brace effectively controls the dynamic response of the structure.
- By comparing the capacity curves of the structures, it can be seen that the SS has a large lateral stiffness resistance and strong lateral force resistance at the elastic stage, and a strong deformability and good ductility in the yield stage, which is favorable for the dissipation of energy.
- According to the appearance process and development sequence of the plastic hinges, it is known that the SS can still resist a certain level of horizontal load when the beam and the brace is in full-section yield, and has a good ductility, indicating that the SS meets multiple aseismic resistance requirements, and has a strong safety reserve which could avoid the brittle damage to the structure. According to the force-bearing characteristics, the beam and brace of the SS can be designed as variable-section member, in order to make full use of materials and save steel.

Acknowledgments

This research described in this paper was financially braceed by the National Natural Science Foundation of China (Grant No. 51608231, 51678221), the National Key R&D Plan-China (Grant No. 2017YFC1500602), Project of Institute of Engineering Mechanics, China Earthquake Administration (Grant No.2017B16) and the Natural Science Foundation of Heilongjiang Province (Grant No.LC2017025). The financial braces offered by these research funds are greatly appreciated by the authors.

References

Binnur G. K. and Secil E.(2005), “Prediction of fracture behavior of steel beam to column connections with weld defect using the SINTAP”, *Engineering Structures*, **27**(1): 760-768.

Fajfar P. (1999), “Capacity spectrum method based on inelastic demand spectra”, *Earthquake Engineering & Structural Dynamics*, **28** (9):979-993.

Fayaz R. R. and Mirjalili M. R.(2018), “Dynamic-based Pushover analysis for one-way plan-asymmetric buildings”, *Engineering Structures*, **163**(1)332-346.

Foulad R.(2015), “On the seismic performance of hat knee bracing system in low-rise multistory steel structures”, *Advances in structural engineering*, **18**(3): 325-338.

Gross J. L.(1998), “A connections model for the seismic analysis of welded steel moment frames”, *Engineering Structures*, **20**(1): 390-397.

Gupta B. and Kunnath S. K.(2000), “Adaptive spectra-based Pushover procedure for seismic evaluation of structures”, *Earthquake Spectra*, **16**(2):367-391.

Kim J. and Seo Y.(2004), “Seismic design of low-rise steel frames with buckling-restrained braces”, *Engineering Structures* , **26**(5): 543-551.

Li S., Zuo Z., Zhai C. and Xie L.(2017), “Comparison of static Pushover and dynamic analyses using RC building shaking table experiment”, *Engineering Structures*, **136**(1):430-440.

Liu H. and Lan Z.(2016), “Seismic response analysis of separated structural systems”, *World earthquake engineering*, **32**(3):7-12.

Liu H., Shao Y., Song J. and Zhao Y.(2015), “Study on stiffness and bearing capacity of composite beams with variable web height”, *Special structures*, **32**(6): 1-6.

Liu Y., Kuang J. and Huang Q.(2018), “Modified spectrum-based Pushover analysis for estimating seismic demand of dual wall-frame systems”, *Engineering Structures*, **165**(1):302-314.

Phaiboon P.(2014), “Cyclic Pushover Analysis procedure to estimate seismic demands for buildings”, *Engineering*

Structures, **66**(5):10-23.
Piotr D. M., Brian M. M. and Robert D. C. (2001), “Earthquake failures of welded building connections”, *International Journal of Solids and Structures*, **38**(1): 2025-2032.
Reza Z. B. and Mohsenali S.(2018), “An energy-based Pushover-analysis with torque-effects in assessment of the structures with asymmetric plan”, *Soil Dynamics and Earthquake Engineering*, **108**(1):58-68.
Torii A. J. and Machado R. D.(2012), “Structural dynamic analysis for time response of bars and trusses using the generalized finite element method”, *Latin American Journal of Solids and Structures*, **9**(3): 309-337.
Vasdravellis G. B., Tan E.L. and Kirkland B.(2015), “Behaviour and design of composite beams subjected to sagging bending and axial compression”, *Journal of Constructional Steel Research*, **110**(1): 29-39.
Yang X., Luo Y. and Shen Z.(2017), “An extended modal Pushover procedure for estimating the in-plane seismic responses of latticed arches”, *Soil Dynamics and Earthquake Engineering*, **93**(1):42-60.
Yin L., Tang G., Li Z., Zhang M. and Feng B. (2018), “Responses of cold-formed steel storage racks with spine bracings using speed-lock connections with bolts I: Static elastic-plastic Pushover analysis”, *Thin-Walled Structures*, **125**(1):51-62.